Microscopy and Microanalysis, **31** (7), 2025, 1560–1562
https://doi.org/10.1093/mam/ozaf048.801

Microscopy AND Microanalysis

Proceedings

Time-Resolved 4D STEM Reveals Facilitated Dynamics in a Multicomponent Metallic Glass Forming Liquid

Shuoyuan Huang[1,2], Shiyi Qin[3], Ludovic Berthier[4,5], Camille Scalliet[6], Victor M. Zavala[3], and Paul M. Voyles[1,*]

[1]*Department of Materials Science and Engineering, University of Wisconsin Madison, Madison, Wisconsin, USA*
[2]*Center for Functional Nanomaterials, Brookhaven National Laboratory, Upton, New York, USA*
[3]*Department of Chemical and Biological Engineering, University of Wisconsin Madison, Madison, Wisconsin, USA*
[4]*Laboratoire Charles Coulomb (L2C), Université de Montpellier, CNRS, Montpellier, France*
[5]*Gulliver, UMR CNRS 7083, ESPCI Paris, PSL Research University, Paris, France*
[6]*Laboratoire de Physique de l'Ecole normale supérieure, ENS, Université PSL, CNRS, Sorbonne Université, Université Paris Cité, Paris, France*
*Corresponding author: paul.voyles@wisc.edu

Deeply supercooled liquids (SCLs) exhibit spatially heterogeneous dynamics where local mobility varies by orders of magnitude even a few nanometers apart as they cool toward the glass transition. Dynamic facilitation theory attributes this heterogeneity to regions of high mobility that facilitate the excitation of dynamics in neighboring areas [1,2]. Experimental evidence for dynamic facilitation have been observed in colloidal systems with video microscopy [3], but individual particle tracking is required, which is unfeasible for more complex three-dimensional liquids.

Time-resolved four-dimensional scanning transmission electron microscopy (4D STEM) has been demonstrated to probe relaxation behaviors in liquids with nanoscale spatial resolution [4]. The time series of diffraction intensity were used to obtain relaxation time scales for different regions. However, rich spatial-temporal correlations in the local dynamics remain largely unexplored, due to the complexity of data. Here, we use the Euler characteristic (EC) [5], a simple yet powerful topological descriptor, to identify spatiotemporal correlative features in time-resolved 4D STEM data, which leads to evidence for dynamic facilitation in a metallic glass forming liquid.

Figure 1 shows the process of experimental acquisition and data analysis. Repeated 4D STEM experiments (Fig. 1a) were performed on a $Pt_{57.5}Cu_{14.5}Ni_{5.5}P_{22.5}$ metallic glass nanowire which was heated *in situ* above its glass transition temperature. This generated a five-dimensional diffracted intensity data $I(x, y, k_r, k_\phi, t_f)$, where x, y are spatial coordinates, k_r, k_ϕ are radial and azimuthal component of the wave vector $\mathbf{k}$, and t_f is the time of acquired frame. To describe the spatiotemporal dynamics, the time autocorrelation function was calculated by

$$g_2(x, y, k_r, k_\phi, t) = \frac{I(x, y, k_r, k_\phi, t_f)I(x, y, k_r, k_\phi, t_f + t)_{t_f}}{I(x, y, k_r, k_\phi, t_f)^2_{t_f}}, \quad (1)$$

where t is elapsed time. The g_2 data hypercube contains information of the time-space behavior of dynamics. An example $g_2(x, y, t)$ data cube at a certain wavevector $\boldsymbol{k}$ is plotted in Fig. 1b. $g_2(x, y)$ data represents an intensity map that depicts the level of correlation at a certain elapsed time t. The correlation intensity map $g_2(x, y)$ at a certain elapsed time t (Fig. 1c) can be transformed into a two-dimensional binary map by applying a filtration threshold. Examples of filtered 2D map at various filtration levels are shown in Fig. 1d. The topology of these resulting 2D shapes is studied by persistent homology [6] with the n-th Betti number β_n denoting the rank of n-th homology group: β_0 is the number of connected components, and β_1 is the number of holes. The EC is then calculated by [7]

$$\chi_{g_2} = \beta_0 - \beta_1. \quad (2)$$

An EC curve summarizing the topology of the $g_2(x, y)$ data at multiple scales is calculated as a function of the filtration level, as shown in Fig. 1d. Since the relaxation dynamics depend on the wave-vector magnitude k_r rather than the scattering angle k_ϕ, the results were calculated individually for all $\boldsymbol{k}$ pixels and then averaged over k_ϕ. The analysis was only performed over the k_r range of the first structure factor peak from 0.32 to 0.56 $Å^{-1}$.

A varying filtration level is necessary at each elapsed time to account for the spatially varying exponential decrease in g_2. The EC curve summarizes the topology of the g_2 data across different filtration levels. Peaks and valleys in the EC curve represent the g_2 values where most regions are situated. Consequently, filtration levels at the maximum EC were used for each time step. Two topological descriptors were calculated: the number density of domains

$$\text{Number density} = \frac{\beta_0|_{\max\chi}}{S}, \quad (3)$$

$$\overline{\text{Domain area}} = \left.\frac{A_f}{\beta_0}\right|_{\max\chi}, \quad (4)$$

where S is the total area of the sample, and the average domain area

where A_f is the area of filtered object. By comparing the experimental results with a synthetic random model and results from an MD simulation [8], we show that the time dependencies of these two descriptors reveal spatiotemporal insight about the dynamic process in the context of DF.

Fig. 2 shows the number density of fast- and slow-relaxing regions as a function of time (normalized by relaxation time τ) in experimental g_2 (panels a, b, d and e) compared with synthetic g_2 data (panel c and f) for which the degree of facilitation is an adjustable parameter. Two key signatures of DF are identified that exist in experiment, MD simulation (not shown), and synthetic model: (1) the plateau in fast domain number density near $t \approx \tau$, which is related to the growth of fast domains as a result of facilitation; and (2) the increase in slow domain number density at times longer than τ, which is a result of percolation of fast domains due to facilitation. Behaviors arising from similar physical process are also found for the domain area metric. It is also evident that both features in number density are stronger for data collected near the structure factor peak, as seen for the data with colder colors in Fig. 2a and 2d. On the other hand, the behavior of the number density depends less on temperature (Fig. 2b and 2e), which is likely due to the narrow temperature range collected.

At k near the structure factor peak, where atomic packing is denser, stronger facilitation may result from stronger bonding, consistent with de Gennes' argument for slow dynamics at the structure factor peak [9]. We have previously shown that different chemical bonding in multicomponent system exhibit decoupled dynamic behavior [4]. This connection between bonding strength and facilitation level potentially links dynamic facilities to dynamic heterogeneity in SCLs. The results suggest the existence of dynamic facilitation in a multicomponent metallic liquid, and that it is stronger for data collected near the structure factor peak, potentially related to longer relaxation times and growing heterogeneity.

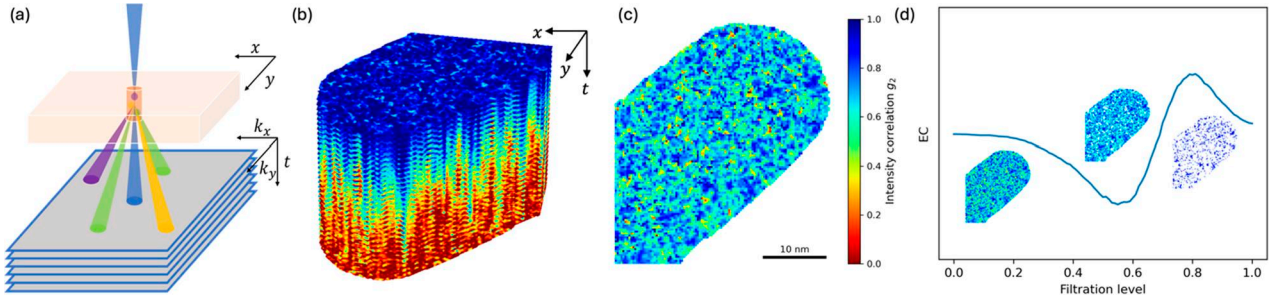

Fig. 1. (a) Schematic illustration time-resolved 4D STEM experiment; (b) Example of $g_2(x, y, t)$ data cube; (c) Example of $g_2(x, y)$ map at certain elapsed time; (d) Illustration of EC curve at different filtration level. Insets are filtered g_2 data object.

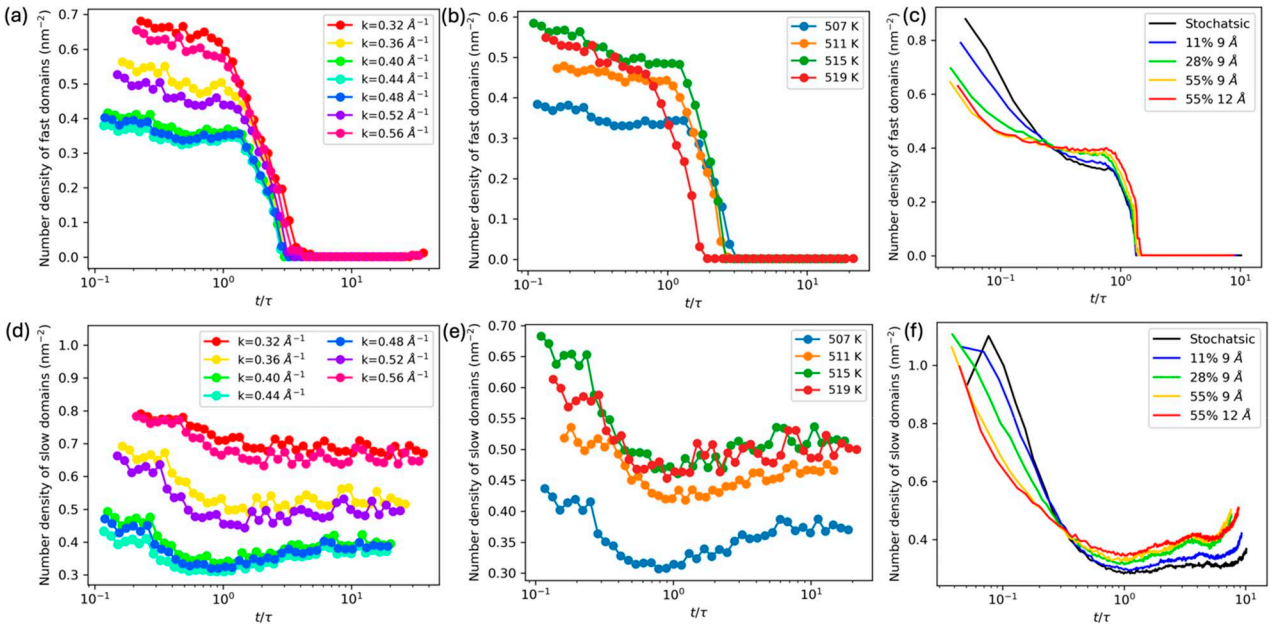

Fig. 2. Number density of fast domains for $Pt_{57.5}Cu_{14.5}Ni_{5.5}P_{22.5}$ nanowires at (a) different k at 507 K and (b) different temperatures at 0.44 Å^{-1}, and (c) for synthetic random models with different levels of dynamic facilitation. The number density of slow domains at (d) different k at 507 K and (e) different temperatures at 0.44 Å^{-1}, and (f) for synthetic random models with different levels of dynamic domains.

References

1. Palmer RG *et al. Phys. Rev. Lett.* (1984) **53** 958–961. https://doi.org/10.1103/PhysRevLett.53.958
2. Garrahan JP and Chandler D. *Proc. Natl. Acad. Sci.* (2003) **100** 9710–9714. https://doi.org/10.1073/pnas.1233719100
3. Gokhale S *et al. Nat. Commun.* (2014) **5** 1–7. https://doi.org/10.1038/ncomms5685
4. Huang S and Voyles PM. *Ultramicroscopy* (2024) **256** 113886. https://doi.org/10.1016/j.ultramic.2023.113886
5. Smith A and Zavala VM. *Comput. Chem. Eng* (2021) **154** 107463. https://doi.org/https://doi.org/10.1016/j.compchemeng.2021.107463
6. Carlsson G. *Bull. Am. Math. Soc.* (2009) **46** 255–308.
7. Adler RJ *et al. arXiv* (2010) arXiv:1003.1001. https://doi.org/10.48550/arXiv.1003.1001
8. Scalliet *et al. Phys. Rev. X* (2022) **12** 41028. https://doi.org/10.1103/PhysRevX.12.041028
9. De Gennes PG. *Physica* (1959) **25** 825–839. https://doi.org/10.1016/0031-8914(59)90006-0